



HAL
open science

Transport properties of polycrystalline p-type SnSe

Selma Sassi, Christophe Candolfi, Jean-Baptiste Vaney, Viktoriia Ohorodniichuk, Philippe Masschelein, Anne Dauscher, Bertrand Lenoir

► **To cite this version:**

Selma Sassi, Christophe Candolfi, Jean-Baptiste Vaney, Viktoriia Ohorodniichuk, Philippe Masschelein, et al.. Transport properties of polycrystalline p-type SnSe. *Materials Today: Proceedings*, 2015, 2 (2), pp.690-698. 10.1016/j.matpr.2015.05.093 . hal-01280800

HAL Id: hal-01280800

<https://hal.science/hal-01280800>

Submitted on 2 Mar 2023

HAL is a multi-disciplinary open access archive for the deposit and dissemination of scientific research documents, whether they are published or not. The documents may come from teaching and research institutions in France or abroad, or from public or private research centers.

L'archive ouverte pluridisciplinaire **HAL**, est destinée au dépôt et à la diffusion de documents scientifiques de niveau recherche, publiés ou non, émanant des établissements d'enseignement et de recherche français ou étrangers, des laboratoires publics ou privés.

Transport properties of polycrystalline *p*-type SnSe

S. Sassi, C. Candolfi, J.-B. Vaney, V. Ohorodniichuk, P. Masschelein, A. Dauscher, B.

Lenoir*

Institut Jean Lamour, UMR 7198 CNRS – Nancy Université – UPVM, Parc de Saurupt,

54042 Nancy, France

*Contact author: bertrand.lenoir@univ-lorraine.fr

Abstract

We report on the transport properties of polycrystalline *p*-type SnSe in a broad temperature range (2 – 800 K) by means of electrical resistivity, thermopower, thermal conductivity, Hall effect and specific heat. The electrical properties confirm the lightly-doped semiconducting nature of SnSe. The low-temperature specific heat data feature an excess contribution, which originates from the low-energy phonon modes characterizing the phonon spectrum of this compound. The thermal conductivity is typical of crystalline solids as shown by pronounced maxima observed at low temperatures. The excellent agreement between the values measured at low and at high temperatures further question the results recently obtained on single crystals.

I. Introduction

Thermoelectric devices, which allow direct solid-state conversion between heat and electricity, have been successfully used for decades in space applications as power supply.^{1,2} Yet, because the maximum efficiency range between 3 and 7%, thermoelectric devices remain so far confined in niche technologies. The emergence of new family of materials that would enable higher conversion efficiency to be achieved could widespread this technology in solid state cooling or power generation applications. The thermoelectric performance of a material at a given temperature T is evaluated with the dimensionless figure of merit ZT defined as $ZT = \alpha^2 T / \rho \kappa$ where α is the Seebeck coefficient or thermopower, ρ is the electrical resistivity and κ is the total thermal conductivity.¹⁻³ Because of their structural simplicity and advantageous electronic band structure, the rocksalt (NaCl-type) IV-VI compounds have focused continuing efforts in optimizing their thermoelectric properties. An impressive amount of literature data on these compounds is available, among which several studies have reported very high ZT values over 1.5 around 800 K in Pb-based alloys.⁴⁻¹⁰

Although SnSe belongs to this family of compounds, it crystallizes in a layered structure described within the orthorhombic space group $Pnma$ (Figure 1) resulting in strongly anisotropic transport properties.^{11,12} While several theoretical and experimental investigations unveiled some of its mechanical, electronic and thermal properties, this binary compound has only recently come to the forefront of research owing to the report of extremely high ZT values of up to 2.6 near 800 K in single crystals.¹³⁻²² These record values mainly arose due to the very low thermal conductivity values measured in this study. This result prompted further investigations aiming at determining whether similar values can be found in polycrystals.^{14,15} However, these studies revealed significantly higher thermal conductivity values with respect

to those found by Zhao *et al.*¹³ resulting in maximum ZT values of 0.5 at 820 K in undoped SnSe and 0.6 at 750 K in $\text{Ag}_{0.01}\text{Sn}_{0.99}\text{Se}$.^{14,15}

Herein, we further explore the transport properties of polycrystalline p -type SnSe by means of electrical resistivity, thermopower, thermal conductivity and specific heat in a broad temperature range (2 – 800 K). Our results further confirm the higher thermal conductivity values reported by other groups either experimentally or theoretically with respect to the results of Zhao *et al.*¹³ The electronic properties at 300 K were modelled within a single parabolic band model from which the hole effective masses are estimated. Besides complementing early studies performed on single crystals, our results may serve as a useful basis for further optimization of the high-temperature thermoelectric properties of p -type SnSe.

II. Experimental details

Polycrystalline samples of SnSe were synthesized by a two-step metallurgical route. As a first step, stoichiometric amounts of pure Sn shots (99.999%) and Se powders (99.999%) were sealed under He/H₂ (90/10%) atmosphere in a quartz tube. The tube was then heated up to 1223 K, kept at this temperature for one day, furnace-cooled to 773 K and finally quenched in room-temperature water. The powders were densified by spark plasma sintering (SPS) at 708 K for 7 minutes under a uniaxial pressure of 50 MPa. Powder x-ray diffraction and scanning electron microscopy were performed to verify the crystal structure and the chemical homogeneity of the sample, respectively. These experiments indicated that SnSe was successfully obtained with only traces of elemental Sn as a secondary phase. Fracture images further confirmed the strong anisotropy of the sample as shown by large areas where a plate-like microstructure is clearly visible.¹⁴

Electrical resistivity, thermopower and thermal conductivity were measured simultaneously below 300 K with the thermal transport option of a physical property measurement system (PPMS, Quantum Design). These measurements were performed on bar-shaped samples of well-defined geometry (typically $2 \times 2 \times 8 \text{ mm}^3$) cut with a diamond wire saw. Four contacts made with copper bars were attached on the samples with conductive silver epoxy solidified by heating the samples up to 130°C . While κ could be measured from 300 K down to 5 K, the highly resistive character of these samples prevented the ρ and α data from being collected below ~ 100 K. Hall effect was measured at 300 K by the ac transport option of a PPMS. A five-point contact method was employed by attaching five copper wires with a minute amount of silver paste. The Hall resistivity ρ_H was obtained after correcting possible misalignment of the contacts following the formula $\rho_H = [\rho_{xy}(+\mu_0 H) - \rho_{xy}(-\mu_0 H)]/2$ where ρ_{xy} is the measured transverse electrical resistivity. Note that, owing to the anisotropic crystal structure of SnSe, all the measurements presented here were carried out on samples cut parallel and perpendicular to the pressing direction. The specific heat was measured between 2 and 300 K on a small sample of approximately 20 mg with the dedicated option of the PPMS using a conventional relaxation method. The low-temperature and high-temperature data were collected on samples coming from the same sample batch.

For comparison purposes, the data measured at high temperatures in Ref. 14 have been added. Not only does this enable a direct comparison between the two sets of data but, in the case of the thermal conductivity, also provides a self-consistent check of the values measured by two different technologies. Because the high-temperature data were described in detail in Ref. 14, we shall here mainly focus our discussion on the low-temperature region.

III. Results and discussion

A. Electronic and galvanomagnetic properties

Figure 2a shows the temperature dependence of the electrical resistivity. ρ strongly decreases with increasing temperature up to 400 K indicative of a semiconducting regime. At this temperature, the upturn and the maximum seen at 500 K might be related to the presence of minute amounts of elemental tin in the sample. At higher temperatures, ρ further decreases up to 800 K where the structural transition sets in.¹³ The high ρ values measured are consistent with a nearly intrinsic or lightly-doped semiconducting state of SnSe. This conclusion is further corroborated by the low hole concentration of $\sim 4 \times 10^{17} \text{ cm}^{-3}$ at 300 K measured in both directions. This concentration is similar to that found by Zhao *et al.*¹³ and by Chen *et al.*¹⁵ Of note, this value also agrees with those obtained by Maier and Daniel on single crystals grown under various experimental conditions.¹⁶ These authors showed that deviations from the ideal stoichiometry may be achieved by varying the growth temperature and/or the annealing temperature and time resulting in hole concentrations ranging between $1.3 \times 10^{17} \text{ cm}^{-3}$ and $1.9 \times 10^{18} \text{ cm}^{-3}$ at 77 K.

The high thermopower values measured are also in agreement with the semiconducting character of SnSe (Figure 2b). The α values rapidly rise with temperature to reach $500 \mu\text{V.K}^{-1}$ around 300 K. Above this temperature, α remains nearly constant up to 500 K before decreasing to reach $330 \mu\text{V.K}^{-1}$ at 800 K.

The combination of the n_H and α data enables estimating the hole density of states effective masses m_d^* . A single parabolic band model was considered due to the non-degenerate character of the transport properties and the large band gap. The former characteristic necessitates taking into account deviations from unity of the Hall factor, which

relates the Hall to the chemical carrier concentration by $n_H = n/r_H$. Within this formalism, n_H , r_H and α express as²³

$$\alpha = \frac{k_B}{e} \left[\frac{(2 + \lambda)F_{1+\lambda}(\eta)}{(1 + \lambda)F_\lambda(\eta)} - \eta \right] \quad (1)$$

$$n_H = 4\pi \left(\frac{2m_d^*k_B T}{h^2} \right)^{3/2} \frac{F_{1/2}(\eta)}{r_H} \quad (2)$$

$$r_H = \frac{3}{2} F_{1/2}(\eta) \left[\frac{(1/2 + 2\lambda)F_{2\lambda-1/2}(\eta)}{(1 + \lambda)^2 F_\lambda^2(\eta)} \right] \quad (3)$$

In these equations, k_B is the Boltzmann constant, e is the elementary charge, h is the Planck constant, λ is a parameter that reflects the type of scattering mechanism of the charge carriers, η is the reduced Fermi level and $F_i(\eta)$ is the Fermi integral of i th order defined by $F_i(\eta) = \int_0^\infty \frac{\xi^i d\xi}{1 + e^{(\xi-\eta)}}$ with ξ being the reduced carrier energy. Chen *et al.*¹⁵ showed that acoustic phonon scattering prevails near room temperature in undoped SnSe. Hence, using $\lambda = 0$ together with the experimental n_H and α values in the above set of equations yield an estimate of m_d^* of $0.7m_0$ and $0.6m_0$ (m_0 is the bare electron mass) in the parallel and perpendicular directions, respectively. These values are consistent with that derived by Chen *et al.*¹⁵ ($0.75m_0$) in both undoped and Ag-doped samples.

B. Thermal properties

The specific heat C_p as a function of temperature is presented in Figure 3a. Around 300 K, the C_p values near the Dulong-Petit limit of $3NR$ where N is the number of atoms per formula unit and R is the gas constant. The low-temperature data, plotted as C_p/T versus T^2

in Figure 3b, can be fitted to the Debye expression $C_p/T = \gamma + \beta T^2$ where γ and β stand for the electronic and phononic contribution, respectively. The best fit to the data yields a γ value indistinguishable from zero to within experimental uncertainty in agreement with the semiconducting character of this compound. The β parameter enables an estimation of the Debye temperature θ_D according to the relation $\theta_D = \left(\frac{12\pi^4 NR}{5\beta} \right)^{\frac{1}{3}}$. In the present case, the value of β gives $\theta_D \approx 208$ K. This value is in good agreement with that derived theoretically by He *et al.*²¹ who found a Debye temperature of 215 K.

The low-energy features of the phonon spectrum usually give rise to specific heat in excess of the Debye contribution. A plot of C_p/T^3 versus T emphasizes this contribution, which shows up as a maximum whose peak temperature and amplitude depends on the system. In general, an increased disorder in the unit cell shifts this maximum toward lower temperatures with a concomitant increase in its amplitude. Such feature has been observed in several families of thermoelectric compounds including cage-like materials such as clathrates or skutterudites and in materials with complex unit cells.²⁴⁻³² SnSe follows this trend as shown in Figure 3c where a pronounced peak centered near 14 K is observed. To investigate in more detail this peak, the C_p/T^3 data were fitted to the sum of a Debye contribution with two additional low-energy Einstein modes to describe the main features of the low-energy phonon spectrum. The Debye background was calculated from our experimental θ_D value. Each Einstein oscillator gives a contribution to the specific heat that can be expressed as

$$C_E = pR \frac{\left(\frac{\hbar\omega_0}{k_B T} \right)^2 e^{\frac{\hbar\omega_0}{k_B T}}}{\left(e^{\frac{\hbar\omega_0}{k_B T}} - 1 \right)^2} \quad (4)$$

In Eq.(4), p is the spectral weight of the oscillator, $\hbar\omega_0$ is the energy of the mode and k_B is the Boltzmann constant. The best fit to the data with $\hbar\omega_0$ and p as free parameters for each mode yield energies of 4.2 and 5.1 meV with oscillator strengths of 0.41 and 0.46, respectively. These two energies, which correspond to Einstein temperatures of 61 and 74 K, agree well with the first modes of the phonon density of states calculated by Carrete *et al.*²² According to these calculations, the lowest energy mode originates from the low-energy optical modes while the second is due to the acoustic modes near the Brillouin zone boundary.²² Note that the latter value is in fact an average of the different phonon modes giving rise to several sharp features in the PDOS spectrum around 5 meV.

Figure 4 shows the temperature dependence of the parallel and perpendicular thermal conductivities. Due to the highly resistive nature of the samples, the electronic contribution is negligible and the data thus entirely reflect the lattice thermal conductivity. These measurements indicate room temperature values of 0.9 and 1.4 W.m⁻¹.K⁻¹ in the parallel and perpendicular direction, respectively. In both directions, the results evidence a pronounced dielectric maximum near 25 K characteristic of crystalline solids. Above this temperature, κ strongly decreases following approximately a T^{-1} law due to increased Umklapp scattering events. These results confirm our high-temperature data (Ref. 14) and are consistent with the values measured by Chen *et al.*¹⁵ and those obtained from *ab-initio* calculations by Carrete *et al.*²² In the latter study, the room-temperature κ_L values computed were 0.55, 1.8 and 0.9 along the a , b and c crystallographic directions, respectively. The very low values observed in the a and b directions originate from the presence of soft acoustic phonon modes that exhibit high Grüneisen parameters.^{13,21,22} High values of this parameter are synonymous with strong anharmonicity of the bonding giving rise to an enhanced phonon-phonon scattering rate and hence, to lower thermal conductivity values.

IV. Conclusion

We reported on the transport properties of polycrystalline SnSe. Our measurements further confirm the high-temperature data reported by several groups. In particular, the thermal conductivity values are significantly higher than those obtained by Zhao *et al.* on single crystals. The thermal transport is characterized by a behavior typical of crystalline solids typified by pronounced dielectric maxima at low temperatures. The low thermal conductivity values measured together with excess specific heat at low temperatures are suggestive of enhanced anharmonicity of the chemical bonding. A better understanding of this anharmonicity might be achieved by investigating the phonon spectrum of this compound. Because the present sample behaves as a lightly-doped or nearly-intrinsic semiconductor, further optimization of the thermoelectric properties may be expected by doping. In addition, the introduction of resonant levels in the band structure, as reported in Tl-doped PbTe,³³⁻³⁴ might be a worthwhile way of research to pursue.

References

- ¹ *Thermoelectrics and its Energy Harvesting*, edited by D. M. Rowe (CRC Press, 2012).
- ² *Thermoelectrics Handbook, Macro to Nano*, edited by D. M. Rowe (CRC Press, Taylor & Francis Group, Boca Raton FL, 2006).
- ³ H. J. Goldsmid in *Thermoelectric Refrigeration* (Temple Press Books, Ltd.: London, 1964).
- ⁴ Y. Pei, X. Shi, A. LaLonde, H. Wang, L. Chen and G. J. Snyder, *Nature* **473**, 66-69 (2011).
- ⁵ K. Biswas, J. He, I. D. Blum, C. I. Wu, T. P. Hogan, D. N. Seidman, V. P. Dravid and M. G. Kanatzidis, *Nature* **489**, 414-418 (2012).
- ⁶ L. D. Zhao, J. He, C. I. Wu, T. P. Hogan, X. Zhou, C. Uher, V. P. Dravid and M. G. Kanatzidis, *J. Am. Chem. Soc.* **134**, 7902-7912 (2012).
- ⁷ H. Wang, E. Schechtel, Y. Pei and G. J. Snyder, *Adv. Ener. Mater.* **3**, 488-495 (2013).
- ⁸ Y. Chen, M. D. Nielsen, Y.-B. Gao, T.-J. Zhu, X. Zhao, J. P. Heremans, *Adv. Ener. Mater.* **2**, 58-62 (2012).
- ⁹ A. D. LaLonde, Y. Pei and G. J. Snyder, *Energy Environ. Sci.* **4**, 2090-2096 (2011).
- ¹⁰ C. M. Jaworski, B. Wiendlocha, V. Jovovic, J. P. Heremans, *Energy Environ. Sci.* **4**, 4155 (2011).
- ¹¹ I. Lefebvre, M. A. Szymanski, J. Olivier-Fourcade and J. C. Jumas, *Phys Rev B* **58**, 1896-1906 (1998).
- ¹² T. Chattopadhyay, J. Pannetier and H. G. Vonschnering, *J. Phys. Chem. Solids* **47**, 879-885 (1986).
- ¹³ L. D. Zhao, S. H. Lo, Y. Zhang, H. Sun, G. Tan, C. Uher, C. Wolverton, V. P. Dravid and M. G. Kanatzidis, *Nature* **508**, 373-377 (2014).
- ¹⁴ S. Sassi, C. Candolfi, J.-B. Vaney, V. Ohorodniichuk, P. Masschelein, A. Dauscher, B. Lenoir, *Appl. Phys. Lett.* **104**, 212105 (2014).

- ¹⁵ C.-L. Chen, H. Wang, Y.-Y. Chen, T. Day, G. J. Snyder, *J. Mater. Chem. A* **2**, 11171 (2014).
- ¹⁶ H. Maier, D. R. Daniel, *J. Elec. Mater.* **6**, 693-704 (1977).
- ¹⁷ J. D. Wasscher, W. Albers, C. Haas, *Solid State Elec.* **6**, 261-264 (1963).
- ¹⁸ W. Albers, C. Haas, H. Ober, G. R. Schodder, J. D. Wasscher, *J. Phys. Chem. Solids* **23**, 215-220 (1962).
- ¹⁹ B. B. Nariya, A. K. Dasadia, M. K. Bhayani, A. J. Patel, A. R. Jani, *Chalco. Lett.* **6**, 549-554 (2009).
- ²⁰ S. Chen, K. Cai, W. Zhao, *Physica B* **407**, 4154-4159 (2012).
- ²¹ X. He, H. Shen, W. Wang, Z. Wang, B. Zhang, X. Li, *J. All. Compd.* **556**, 86-93 (2013).
- ²² J. Carrete, N. Mingo, S. Curatolo arXiv:1406.3532v1.
- ²³ V. I. Fistul, *Heavily Doped Semiconductors* (Plenum Press, New York, 1969).
- ²⁴ U. Aydemir, C. Candolfi, A. Ormeci, Y. Oztan, M. Baitinger, N. Oeschler, F. Steglich, Yu. Grin, *Phys. Rev. B* **84**, 195137 (2011).
- ²⁵ U. Aydemir, C. Candolfi, H. Borrmann, M. Baitinger, A. Ormeci, W. Carrillo-Cabrera, C. Chubilleau, B. Lenoir, A. Dauscher, N. Oeschler, F. Steglich, Yu. Grin, *Dalton Trans.* **39**, 1078-1088 (2010).
- ²⁶ C. Candolfi, U. Aydemir, A. Ormeci, W. Carrillo-Cabrera, U. Burkhardt, M. Baitinger, N. Oeschler, F. Steglich, Yu. Grin, *J. Appl. Phys.* **110**, 043715 (2011).
- ²⁷ K. Suekuni, M. A. Avila, K. Umeo, T. Takabatake, *Phys. Rev. B* **75**, 195210 (2007).
- ²⁸ M. A. Avila, K. Suekuni, K. Umeo, H. Fukuoka, S. Yamanaka, T. Takabatake, *Phys. Rev. B* **74**, 125109 (2006).
- ²⁹ K. Dimitrov, M. E. Manley, S. M. Shapiro, J. Yang, W. Zhang, L. D. Chen, Q. Jie, G. Ehlers, A. Podlesnyak, J. Camacho, Q. Li, *Phys. Rev. B* **82**, 174301 (2010).
- ³⁰ M. A. Avila, K. Suekuni, K. Umeo, H. Fukuoka, S. Yamanaka, T. Takabatake, *Appl. Phys.*

Lett. **92**, 041901 (2008).

³¹ B. C. Melot, R. Tackett, J. O'Brien, A. L. Hector, G. Lawes, R. Seshadri, A. P. Ramirez, Phys. Rev. B **79**, 224111 (2009).

³² T. Zhou, M. Colin, C. Candolfi, C. Boulanger, A. Dauscher, E. Santava, J. Hejtmanek, P. Baranek, R. Al Rahal Al Orabi, M. Potel, B. Fontaine, P. Gougeon, R. Gautier, B. Lenoir, Chem. Mater. DOI: 10.1021/cm5016367 (2014).

³³ J. P. Heremans, V. Jovovic, E. S. Toberer, A. Sarmat, K. Kurosaki, A. Charoenphakdee, S. Yamanaka, and G. J. Snyder, Science **321**, 554 (2008).

³⁴ J. P. Heremans, B. Wiendlocha, and A. M. Chamoire, Energy Environ. Sci. **5**, 5510 (2012).

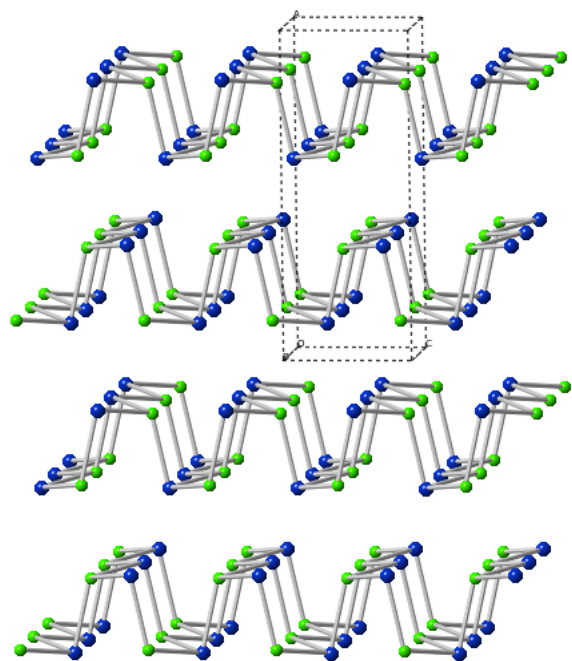
Figure captions

Figure 1: Crystal structure of SnSe along the b (a) and c (b) axis. In each panel, the primitive unit cell is shown. Blue and green spheres stand for Sn and Se atoms, respectively.

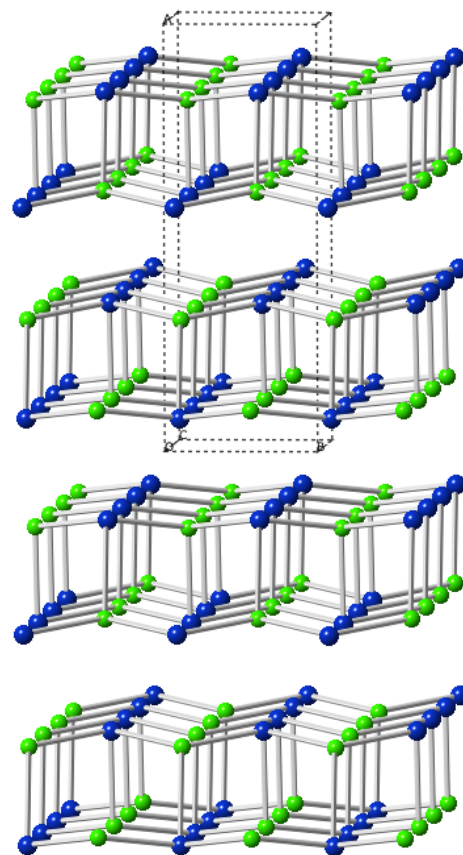
Figure 2: Temperature dependence of the (a) electrical resistivity ρ and (b) thermopower α of SnSe measured parallel (round symbol) and perpendicular (triangle symbol) to the pressing direction.

Figure 3: (a) Temperature dependence of the specific heat C_p . The solid black line stands for the Dulong-Petit limit $3NR$. The anomaly at 508 K corresponds to the melting temperature of elemental tin while that around 800 K might be related to the structural transition. The data around 300 K from the low-temperature measurement have been removed to the extrinsic contribution of the grease used to glue the sample to the puck. (b) Data plotted as C_p/T versus T^2 . The solid black line stands for the best fit to the data (performed between 4 and 20 K²) according to the relation $C_p/T = \gamma + \beta T^2$. (c) C_p data plotted as C_p/T^3 versus T to highlight the excess specific heat due to low-energy phonon modes. The Debye background (square symbol) has been calculated using the experimental Debye temperature of 208 K.

Figure 4: Temperature dependence of the thermal conductivity κ measured parallel (round symbol) and perpendicular (triangle symbol) to the pressing direction.



(a)



(b)

Figure 1

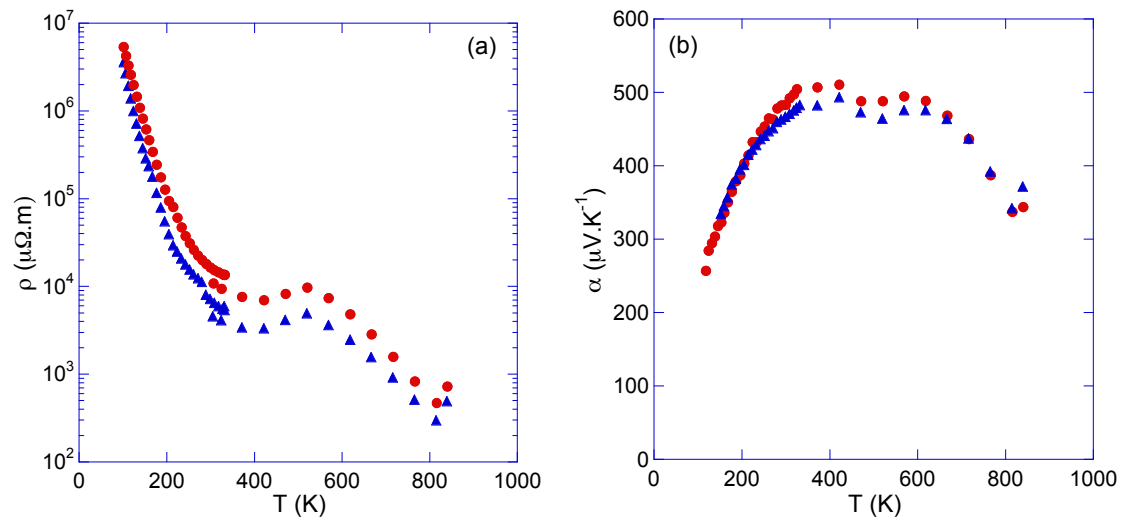


Figure 2

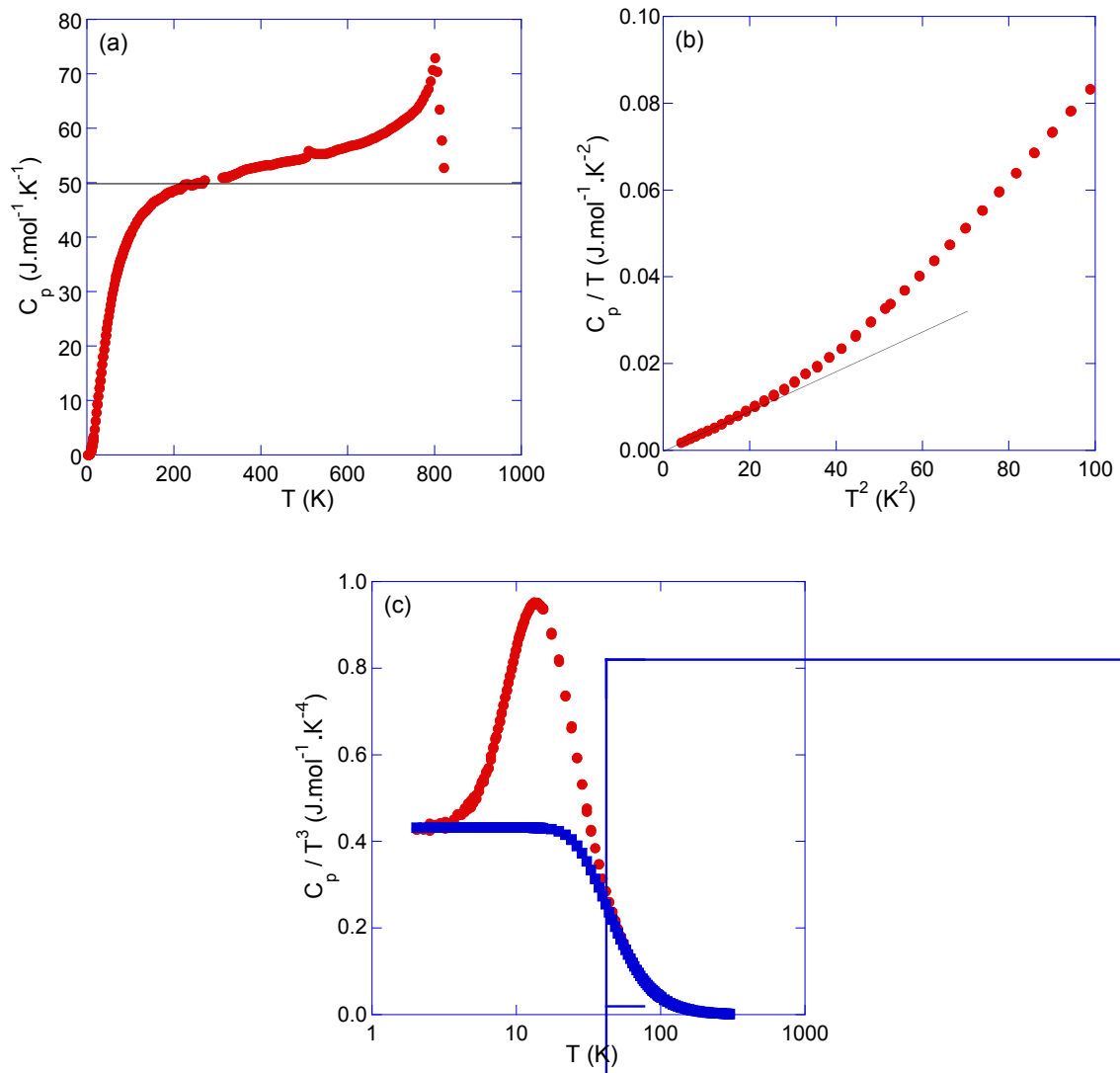


Figure 3

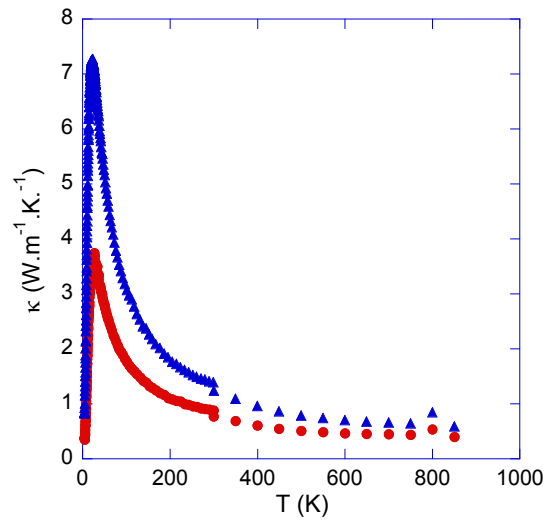


Figure 4